Pulse evolution and plasma-wave phase velocity in channel-guided laser-plasma accelerators

C. Benedetti,[1,*] F. Rossi,[2] C. B. Schroeder,[1] E. Esarey,[1] and W. P. Leemans[1]
[1]*Lawrence Berkeley National Laboratory, Berkeley, California 94720, USA*
[2]*University of Bologna and INFN, Via Irnerio 46, 40126, Bologna, Italy*
(Received 18 December 2014; published 31 August 2015)

The self-consistent laser evolution of an intense, short-pulse laser exciting a plasma wave and propagating in a preformed plasma channel is investigated, including the effects of pulse steepening and energy depletion. In the weakly relativistic laser intensity regime, analytical expressions for the laser energy depletion, pulse self-steepening rate, laser intensity centroid velocity, and phase velocity of the plasma wave are derived and validated numerically.

DOI: 10.1103/PhysRevE.92.023109 PACS number(s): 52.38.Kd, 52.38.Hb

I. INTRODUCTION

Understanding the propagation of short and intense laser pulses in a plasma is a topic of fundamental importance in the field of laser-plasma interactions. For example, in laser-plasma accelerators (LPAs) [1], which have demonstrated the production of multi-GeV electron bunches in cm-scale plasmas [2–4], the dynamics of electron bunch production and acceleration is strongly affected by the properties of the laser-generated plasma wave. More specifically, the plasma-wave velocity determines the dephasing length (distance for a relativistic particle to move out of an accelerating phase of the plasma wave) and, hence, the maximum energy gain for the electrons [1], as well as the threshold for self-injection of background plasma electrons [5]. The plasma-wave velocity driven by a short and intense laser pulse is related to the laser driver and background plasma density properties. Unfortunately, a general analytical theory describing, in three dimensions (3D), the phase velocity and its dependence on the laser-plasma parameters is lacking. However, a calculation of this and other quantities (such as laser energy depletion rate, self-steepening rate, and laser centroid velocity) characterizing the laser evolution in an underdense plasma is essential for the design and optimization of present and future LPA experiments.

In an LPA, the plasma wave (or wakefield) generated by the laser driver is the result of the gradient in laser field energy density providing a force (i.e., the ponderomotive force) that creates a space charge separation between the plasma electrons and the neutralizing ions. Efficient plasma-wave excitation requires a laser driver with a pulse length $L \sim k_p^{-1}$, where $k_p = \omega_p/c$, c being the speed of light in vacuum, and $\omega_p = (4\pi n_0 e^2/m)^{1/2}$ the electron plasma frequency for a plasma with density n_0 (m and e are, respectively, the electron mass and charge). For a fixed pulse length, the wakefield amplitude depends on the amplitude of the peak normalized laser vector potential defined as $a_0 = eA_0/mc^2$, where A_0 is the peak amplitude of the laser vector potential. For a linearly polarized pulse $a_0^2 \simeq 7.32 \times 10^{-19}(\lambda_0[\mu\mathrm{m}])^2 I_0[\mathrm{W/cm^2}]$ with $\lambda_0 = 2\pi/k_0$ the laser wavelength and I_0 the peak intensity. In the limit $a_0 \ll 1$ the phase velocity of the plasma wave, $v_p = c\beta_p$, is equal to the group velocity of the laser, $v_g = c\beta_g$, namely $\beta_p \simeq \beta_g \simeq 1 - k_p^2/2k_0^2$ (or, introducing the Lorentz factor for the velocities, $\gamma_p \simeq \gamma_g \simeq k_0/k_p$) [1]. Current LPA experiments operate at relativistic intensities $I_0 \gtrsim 10^{18}$ W/cm^2, corresponding to $a_0 \gtrsim 1$ with $\lambda_0 \simeq 1$ μm. As shown in Refs. [5–8], in this nonlinear regime, the assumption that the wake phase velocity equals the group velocity of the laser ($\beta_p \simeq \beta_g$) is a poor approximation.

In Ref. [8], Schroeder *et al.* analyzed, for the one-dimensional (1D) case, the propagation in underdense plasmas of high intensity ($a_0 \sim 1$) laser pulses. Calculations for the nonlinear intensity transport and group velocities of the laser pulse, and for the nonlinear phase velocity of the excited plasma wave are presented. It was shown that, in the weakly relativistic regime, $a_0 < 1$, the wake phase velocity is approximately the intensity transport velocity, namely $\gamma_p \simeq (k_0/k_p)[1 + 0.1\,a_0^2]$ (assuming a resonant Gaussian laser pulse). In the nonlinear regime, $a_0 > 1$, the phase velocity depends on the details of laser evolution (laser self-steepening, redshifting, and depletion). More specifically, the phase velocity is initially (i.e., in the early stages of the laser-plasma interaction, before significant depletion takes place) dominated by the nonlinear increase in the plasma wavelength owing to the laser steepening. For instance, if $a_0 \gg 1$, and for a resonant Gaussian pulse, the phase velocity of the peak accelerating field in the m_p-th plasma period behind the driver is [8] $\gamma_p \simeq 0.45(k_0/k_p)m_p^{-1/2}$.

In 3D, approximate expressions for the wake phase velocity valid in limited regions of the parameter space have been proposed. For instance, in Ref. [7], Lu *et al.* used particle-in-cell (PIC) simulations to estimate a constant phase velocity $\gamma_p \simeq k_0/\sqrt{3}k_p$ in the bubble regime [9]. In Ref. [5], Benedetti *et al.* showed, also by means of PIC simulations, that for an intense laser ($a_0 \gtrsim 3$) impinging on a (transversally) uniform plasma the corresponding bubble wake phase velocity is not constant during laser propagation in the plasma. However, the minimum phase velocity measured at the center of the bubble wake, $\gamma_p^{(\mathrm{min})}$, is independent of the laser intensity and follows the (empirical) scaling law $\gamma_p^{(\mathrm{min})} \simeq 2.4(k_0/k_p)^{1/2}$.

In this paper, we investigate, in 3D, the propagation of an intense, short-pulse laser in a preformed parabolic plasma channel. We analytically derive in the weakly relativistic regime, $a_0 < 1$, expressions for the laser energy depletion rate, the laser self-steepening rate, the intensity centroid transport velocity, and the phase velocity of the excited plasma wave, valid in the early stages of the laser-plasma interaction (i.e., before significant depletion takes place). These are

*cbenedetti@lbl.gov

calculated by using an envelope description for the laser pulse and the linearized quasistatic approximation for the (cold, collisionless) plasma response. The analytical solutions are shown to be in good agreement with simulation results obtained with the 2D-cylindrical, ponderomotive PIC code INF&RNO [10,11]. We find that the correct expressions, valid in 3D, characterizing the laser evolution and the plasma-wave phase velocity cannot be inferred from 1D results, and that the difference between 1D and 3D results is not simply given by a predetermined geometric factor. This is due to the interplay between longitudinal and transverse effects in the laser evolution, which, in turn, depends on the functional form of the laser intensity profile. In fact, we find that, for a laser pulse with a longitudinal and transverse Gaussian intensity profile in the limit of a very broad pulse, the expression for the energy depletion, self-steepening rate, and intensity transport velocity are different, in general, from the corresponding expressions obtained in the 1D case discussed in Refs. [8,12], while the 3D expression for the phase velocity reduces to the 1D case. We also study the dependence of the phase velocity on laser driver evolution. In this respect, we identify and discuss the role of transverse pulse evolution (due to mismatched propagation, self-focusing, or plasma-wave guiding) and longitudinal evolution (self-steepening, energy depletion, and redshifting).

The paper is organized as follows. In Sec. II we describe the basic equations for the laser evolution and for the plasma response. In Sec. III we derive the analytical expressions for the laser energy depletion, the self-steepening rate, and the laser intensity centroid velocity. Analytical results are compared with PIC simulations results. Calculations and numerical results for the phase velocity of the laser-driven plasma wave are presented in Sec. IV. Conclusions are presented in Sec. V.

II. LASER EVOLUTION AND PLASMA-WAVE EXCITATION IN THE WEAKLY RELATIVISTIC REGIME

We consider a linearly polarized laser pulse propagating in a parabolic plasma channel with a transverse density distribution, $n_0(r)$, parametrized as

$$n_0(r)/n_{0,0} = 1 + \alpha r^2, \tag{1}$$

where r is the transverse coordinate, $n_{0,0}$ is the on-axis (i.e., $r = 0$) electron plasma density, and α is a parameter describing the depth of the channel ($\alpha = 0$ corresponds to a transversally uniform plasma). Throughout the paper we use dimensionless units, normalizing the time to ω_p^{-1} (plasma frequency corresponding to the on-axis density $n_{0,0}$), and the lengths to $k_p^{-1} = c/\omega_p$.

The laser pulse is represented via the transverse component of its (normalized) vector potential, $A_\perp$, according to

$$a_\perp(\zeta,r,s) \equiv \frac{eA_\perp}{mc^2} = \frac{\hat{a}(\zeta,r,s)}{2}\exp\left(i\frac{k_0}{k_p}\zeta\right) + \text{c.c.}, \tag{2}$$

where $\hat{a}(\zeta,r,s)$ is the (complex) laser pulse envelope, and the exponential term describes the (fast) laser oscillations. In Eq. (2) we introduced the variables $\zeta = z - t$ and $s = t$, which are, respectively, the longitudinal comoving variable and the propagation distance. Given the transverse component of the vector potential, the longitudinal component can be derived from the Coulomb gauge condition, $\nabla \cdot \mathbf{a} = 0$. Assuming a short-pulse laser plasma interaction, i.e., a pulse length $\sim k_p^{-1}$ and propagation in an underdense plasma such that $k_p/k_0 \ll 1$ [this condition enables a separation between fast, $(ck_0)^{-1}$ (laser oscillation), and slow, $\sim (ck_p)^{-1}$ (laser envelope variation and plasma oscillation), time scales], the wave equation for the laser envelope reads [1]

$$\left[\nabla_\perp^2 + 2\left(i\frac{k_0}{k_p} + \frac{\partial}{\partial\zeta}\right)\frac{\partial}{\partial s}\right]\hat{a} = \rho\hat{a}, \tag{3}$$

where $\rho = n(\zeta,r)/[n_{0,0}\gamma(\zeta,r)]$ is the normalized proper density, $n(\zeta,r)$ and $\gamma(\zeta,r)$ being, respectively, the electron density (including the laser-induced perturbation) at a given location and the relativistic factor associated with the local plasma fluid velocity. Associated with Eq. (3) is the following adiabatic invariant (wave action) [13]:

$$\mathcal{A} = \int d\zeta \int dr\, r\left[|\hat{a}|^2 + i\frac{k_p}{k_0}\left(\hat{a}\frac{\partial\hat{a}^*}{\partial\zeta} - \hat{a}^*\frac{\partial\hat{a}}{\partial\zeta}\right)\right], \tag{4}$$

such that $\partial_s\mathcal{A} = 0$.

In the following we will consider as an initial condition a laser pulse with a transverse Gaussian profile, namely

$$\hat{a}(\zeta,r,s=0) = a_0\exp\left(-r^2/w_0^2\right)f(\zeta), \tag{5}$$

where a_0 is the normalized field strength, w_0 is the laser spot, and $f(\zeta)$ describes the longitudinal (temporal) profile of the laser [$0 \leqslant f(\zeta) \leqslant 1$]. The laser pulse defined in Eq. (5) is (linearly) matched in the parabolic channel given by Eq. (1), i.e., it propagates without spot (and intensity) oscillations, if $\alpha = 4/w_0^4$. This is true in the low-intensity and low-power limit, namely $a_0 \ll 1$ and $P/P_c = w_0^2a_0^2/32 \ll 1$ (P and $P_c[\text{GW}] \simeq 17k_0^2/k_p^2$ being, respectively, the laser power and the critical power for self-focusing) [1]. If the laser intensity and/or power are not negligible (i.e., $a_0 \sim 1$ and/or $P/P_c \sim 1$), the matching condition needs to be modified to take into account plasma-wave guiding and relativistic self-focusing effects as discussed in Ref. [14]. For simplicity, in the remainder of the paper we will consider a linearly matched laser pulse.

For a slowly varying laser envelope, namely $|(k_0/k_p)\hat{a}| \gg |\partial_\zeta\hat{a}|$, and in the early stages of the laser-plasma interaction, the leading order term describing the evolution of the envelope is given by $\partial_s\hat{a} \simeq (k_p/k_0)[\rho\hat{a} - \nabla_\perp^2\hat{a}]/(2i)$. Therefore, we have $2\partial_{s,\zeta}^2\hat{a} \simeq -i(k_p/k_0)\partial_\zeta[\rho\hat{a} - \nabla_\perp^2\hat{a}]$, and so Eq. (3) can be approximated as [15]

$$\frac{\partial\hat{a}}{\partial s} \simeq -\frac{i}{2}\frac{k_p}{k_0}\left[\rho\hat{a} - \nabla_\perp^2\hat{a} + i\frac{k_p}{k_0}\partial_\zeta(\rho\hat{a} - \nabla_\perp^2\hat{a})\right]. \tag{6}$$

For any given laser pulse configuration, the evaluation of the proper density requires solving Maxwell's equations coupled with the cold plasma fluid equations, exploiting the quasistatic approximation (i.e., we assume that individual plasma particles are passed over by the laser pulse and the associated wake in a short time compared with the time over which the laser pulse, or the wake, evolve) [16–18]. In the nonlinear (relativistic) regime, $|\hat{a}|^2 \gtrsim 1$, the proper density can be evaluated numerically. Analytical solutions can be obtained in the weakly relativistic limit, $|\hat{a}|^2 < 1$, where the laser contribution can be treated as a perturbation. In this limit,

we have

$$\rho(\zeta,r) = \rho_0(r) + \delta\rho(\zeta,r), \tag{7}$$

where $\rho_0(r) = n_0(r)/n_{0,0}$ is the unperturbed background density [in our case the parabolic plasma channel Eq. (1)], and the laser-induced perturbation, $\delta\rho$, satisfies [1,19]

$$\left(\frac{\partial^2}{\partial\zeta^2} + 1\right)\delta\rho = -(1-\nabla_\perp^2)\frac{|\hat{a}|^2}{4}. \tag{8}$$

In the derivation of Eq. (8) we assumed a broad plasma channel [i.e., $\alpha \ll 1$ for the background plasma density Eq. (1)]. The Green function solution to Eq. (8), valid at early times of the laser-plasma interaction, when the laser envelope is described by Eq. (5), reads

$$\delta\rho(\zeta,r) = \frac{a_0^2}{4}\left[1 + \frac{8}{w_0^2}\left(1 - \frac{2r^2}{w_0^2}\right)\right]e^{-2r^2/w_0^2} \times \int_\zeta^\infty d\zeta' \sin(\zeta-\zeta') f^2(\zeta'). \tag{9}$$

The self-consistent coupling of the laser-driven density perturbation, Eq. (9), to the laser evolution, Eq. (3), describes the laser propagation as discussed in Sec. III.

III. CHARACTERIZATION OF LASER PROPAGATION: ENERGY DEPLETION RATE, SELF-STEEPENING RATE, AND INTENSITY CENTROID VELOCITY

In this section we present analytical expressions, valid at early times of the laser-plasma interaction, in 3D and in the weakly relativistic limit, for three quantities characterizing the propagation of a short and intense laser pulse matched in a parabolic plasma channel, namely the energy depletion rate, laser self-steepening rate, and intensity centroid velocity. Analytical results obtained for a laser pulse with a Gaussian longitudinal and transverse intensity profile are compared with numerical results performed with the ponderomotive code INF&RNO.

A. Laser energy depletion rate

During propagation, the laser driver deposits its energy into the plasma, where a wakefield is created, by means of the transverse plasma current associated with the electron quiver motion in the laser field. This current will do work extracting energy from the laser pulse. An expression for the normalized laser energy, $\mathcal{E}$, as a function of the laser envelope is given by

$$\mathcal{E} = \int d\zeta \int dr\, r\left[\left|\left(1 - i\frac{k_p}{k_0}\frac{\partial}{\partial\zeta}\right)\hat{a}\right|^2 + \frac{1}{2}\left(\frac{k_p}{k_0}\right)^2\left|\frac{\partial\hat{a}}{\partial r}\right|^2\right], \tag{10}$$

where the integral is taken over the whole laser domain. Note that, with the definition of $\mathcal{E}$ given above, the laser energy in physical units is $U_{\rm laser} = (m^2c^4k_0^2/4e^2k_p^3)\mathcal{E}$. The evolution equation for the normalized energy Eq. (10) can be obtained by using Eq. (3), rewritten as $\partial_s[1 - i(k_p/k_0)\partial_\zeta]\hat{a} = -i(k_p/k_0)[\rho\hat{a} - \nabla_\perp^2\hat{a}]/2$, and by making use of the operatorial expansion Eq. (6):

$$\frac{\partial\mathcal{E}}{\partial s} \simeq -\frac{k_p^2}{2k_0^2}\int d\zeta\int dr\, r\frac{\partial\rho}{\partial\zeta}|\hat{a}|^2 + i\frac{k_p^3}{4k_0^3}\int d\zeta\int dr\, r\frac{\partial\rho}{\partial r}\left[\frac{\partial\hat{a}}{\partial r}\hat{a}^* - \hat{a}\frac{\partial\hat{a}^*}{\partial r}\right], \tag{11}$$

where terms $O[(k_p/k_0)^4]$ have been neglected. We note that Eq. (11) is valid at early times of the laser-plasma interaction for any laser intensity. If we assume for $\hat{a}$ the Gaussian laser envelope defined in Eq. (5), we have that the second integral in Eq. (11) vanishes [since $\hat{a} = \hat{a}^*$, then $(\partial_r\hat{a})\hat{a}^* = \hat{a}(\partial_r\hat{a}^*)$]. With this assumption the expression for the initial rate of change of the laser energy Eq. (11) then reads [8,20]

$$\left.\frac{\partial\mathcal{E}}{\partial s}\right|_{s=0} \simeq -\frac{k_p^2}{2k_0^2}\int d\zeta\int dr\, r\frac{\partial\rho}{\partial\zeta}|\hat{a}|^2. \tag{12}$$

For a short laser pulse $\partial_\zeta\rho > 0$ in the region of the driver, yielding $\partial_s\mathcal{E}|_{s=0} < 0$, and so energy is extracted from the laser.

The mean laser wave number (normalized to the initial value) can be expressed as a function of the normalized energy and the wave action as $\langle k/k_0\rangle = \mathcal{E}/\mathcal{A}$. From action conservation we have that $\mathcal{A}\,\partial_s\langle k/k_0\rangle \simeq \partial_s\mathcal{E}$, and so, as the laser depletes, the mean wave number decreases (redshifts). The rate of redshifting equals the rate of energy depletion [8,21].

An analytical expression for the initial (i.e., at early times) laser depletion rate can be obtained in the mildly relativistic regime for a laser with a transverse Gaussian intensity profile matched in a parabolic plasma channel, where the proper density can be expressed as in Eq. (7). We have $\partial_\zeta\rho = \partial_\zeta\delta\rho$, where $\delta\rho$ is given in Eq. (9), and so the initial rate of change of the laser energy is

$$\left.\frac{\partial\mathcal{E}}{\partial s}\right|_{s=0} \simeq -\frac{k_p^2}{k_0^2}\frac{a_0^4w_0^2}{64}\left(1 + \frac{4}{w_0^2}\right)\mathcal{F}, \tag{13}$$

where $\mathcal{F}$, which depends only on the longitudinal profile of the laser pulse, is defined as

$$\mathcal{F} = \int_{-\infty}^{+\infty} d\zeta\int_\zeta^\infty d\zeta'\cos(\zeta-\zeta')f^2(\zeta)f^2(\zeta'). \tag{14}$$

For a laser pulse with a longitudinal Gaussian intensity profile, namely $f(\zeta) = \exp(-\zeta^2/L^2)$, where L is the pulse length, the initial (normalized) laser pulse energy is

$$\mathcal{E}_0 \simeq \sqrt{\frac{\pi}{2}}La_0^2\frac{w_0^2}{4}, \tag{15}$$

where we assumed $L \gg k_p/k_0$, and $w_0 \gg k_p/k_0$, and

$$\mathcal{F} = \frac{\pi}{4}L^2\exp(-L^2/4). \tag{16}$$

Using Eqs. (13), (15), and (16), we obtain the following expression for the initial laser energy depletion rate for a matched bi-Gaussian laser driver,

$$\eta_\mathcal{E} \equiv \frac{1}{\mathcal{E}_0}\left.\frac{\partial\mathcal{E}}{\partial s}\right|_{s=0} \simeq -\frac{1}{32}\sqrt{\frac{\pi}{2}}\frac{k_p^2}{k_0^2}a_0^2\left(1 + \frac{4}{w_0^2}\right)L\,e^{-L^2/4}. \tag{17}$$

An expression for $\eta_\mathcal{E}$ for a half-sine longitudinal laser profile can be found in Ref. [22]. The laser energy pump depletion

length may be defined as $L_{pd} = -\eta_{\mathcal{E}}^{-1}$ [i.e., the initial laser energy evolution is $\mathcal{E}(s)/\mathcal{E}_0 \simeq 1 - s/L_{pd}$, for $s/L_{pd} \ll 1$].

In the very broad pulse (and channel) limit, $w_0^2 \gg 4$, the energy depletion rate is

$$\eta_{\mathcal{E}}^{(\text{3D, broad pulse})} \simeq -\frac{1}{32}\sqrt{\frac{\pi}{2}}\frac{k_p^2}{k_0^2}a_0^2 L\, e^{-L^2/4}. \tag{18}$$

In 1D, the energy depletion rate is [12] $\eta_{\mathcal{E}}^{(\text{1D})} = 2\eta_{\mathcal{E}}^{(\text{3D, broad pulse})}$. The difference between the 1D result and 3D broad pulse result is due to the fact that, in 3D, the laser intensity, and so the transverse current that mediates the energy exchange between the laser and the plasma, is transversally changing due to the laser radial profile, while, in 1D, no transverse laser envelope effects are included. As a consequence, the exact value of the ratio $\eta_{\mathcal{E}}^{(\text{1D})}/\eta_{\mathcal{E}}^{(\text{3D, broad pulse})}$ depends on the details of the transverse intensity distribution. Namely, if the initial laser envelope is described by $a(\zeta,r,s=0) = a_0 g(r) f(\zeta)$, where $g(r)$ is a generic (smooth) function [we assume that $g(r)$ satisfies $g(0) = 1$, and $\int dr\, r\, g^2(r) < +\infty$ (finite laser power)], we have that $\eta_{\mathcal{E}}^{(\text{1D})}/\eta_{\mathcal{E}}^{(\text{3D, broad pulse})} \simeq \int dr\, r\, g^2(r)/\int dr\, r\, g^4(r)$.

We compared the prediction for the initial energy depletion rate Eq. (17) with numerical results obtained with the 2D-cylindrical, ponderomotive, quasistatic PIC code INF&RNO [10,11]. The resolution of the computational grid used for the numerical calculations was $\Delta z = 1/40$ (longitudinal direction), and $\Delta r = 1/30$ (transverse [radial] direction). The electron plasma distribution was represented with five numerical particles per (transverse) cell. The time step for the laser envelope advance was $\Delta s = 0.2$. The error tolerance in the iterative quasistatic solver was set to 10^{-6}. Numerical parameters have been varied to check for numerical convergence. The numerical results are presented in Fig. 1, where we show the initial energy depletion rate as a function of the laser spot, w_0, for different values of the normalized laser strength: $a_0 = 0.1$ (red circles), $a_0 = 0.2$ (green dots), and $a_0 = 0.5$ (blue circles). The longitudinal laser profile is Gaussian with $L = 2$, and $k_0/k_p = 20$. The black dotted lines are the theoretical predictions Eq. (17) for the three laser intensities. The PIC results are in good agreement with theory. The discrepancy between numerical and theoretical energy depletion rate observed at higher laser intensities can be ascribed to the fact that the linear description for the wake amplitude [see Eqs. (7) and (8)] loses its validity.

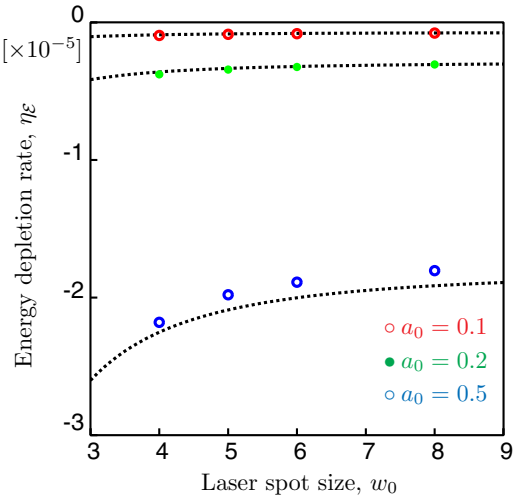

FIG. 1. (Color online) Initial energy depletion rate, $\eta_{\mathcal{E}}$, as a function of the laser spot, w_0, for different values of the normalized laser strength, $a_0 = 0.1$ (red circles), $a_0 = 0.2$ (green dots), and $a_0 = 0.5$ (blue circles). The longitudinal laser profile is Gaussian with $L = 2$, and $k_0/k_p = 20$. The black dotted lines are the theoretical predictions Eq. (17).

B. Laser self-steepening rate

The laser self-steepening of a short laser pulse can be described using the integrated normalized intensity of the laser pulse [8,20,23], defined as

$$\mathcal{Q} = \int d\zeta \int dr\, r|\hat{a}|^2. \tag{19}$$

Alternatively, the self-steepening rate can be studied by examining the skewness of the laser energy distribution, as shown in Ref. [24]. The initial rate of change of $\mathcal{Q}$ is obtained by means of the operatorial expansion Eq. (6). We obtain

$$\frac{\partial \mathcal{Q}}{\partial s} \simeq \frac{k_p^2}{2k_0^2}\int d\zeta \int dr\, r\frac{\partial \rho}{\partial \zeta}|\hat{a}|^2. \tag{20}$$

We note that for a matched laser pulse (i.e., with flat phase fronts) $\partial_s \mathcal{Q} = -\partial_s \mathcal{E}$. We recall that for a short laser pulse matched in a plasma channel $\partial_s \mathcal{E} < 0$, then, as the laser depletes, the quantity $\mathcal{Q}$ increases. An increase in the value of $\mathcal{Q}$ is related, as in 1D, to the increase of the peak laser normalized field strength, a_0 (i.e., laser self-steepening). In fact, owing to the transverse (radial) integral in the definition of $\mathcal{Q}$, the evolution of this quantity is rather insensitive to the transverse redistribution of the laser energy from laser (self-) focusing and/or diffraction, but is sensitive to longitudinal pulse evolution.

In the mildly relativistic limit, and for the Gaussian laser pulse defined in Eq. (5), assuming, as before, matched propagation in a parabolic plasma channel and a longitudinal Gaussian intensity distribution, $f(\zeta) = \exp(-\zeta^2/L^2)$, we obtain the following expression for the initial self-steepening rate:

$$\eta_{\mathcal{Q}} \equiv \frac{1}{\mathcal{Q}_0}\frac{\partial \mathcal{Q}}{\partial s}\bigg|_{s=0} \simeq \frac{1}{32}\sqrt{\frac{\pi}{2}}\frac{k_p^2}{k_0^2}a_0^2\left(1+\frac{4}{w_0^2}\right)L\, e^{-L^2/4}, \tag{21}$$

where $\mathcal{Q}_0 = (\pi/2)^{1/2} L a_0^2 w_0^2/4$. Note that $\eta_{\mathcal{Q}} = -\eta_{\mathcal{E}}$.

We compared the prediction for the initial laser self-steepening rate Eq. (21) with quasistatic PIC results obtained with the code INF&RNO. Simulation results are presented in Fig. 2, where we show the initial self-steepening rate as a function of the laser spot, w_0, for different values of the normalized laser strength: $a_0 = 0.1$ (red circles), $a_0 = 0.2$ (green dots), and $a_0 = 0.5$ (blue circles). The longitudinal laser profile is Gaussian with $L = 2$, and $k_0/k_p = 20$. The black dotted lines are the theoretical predictions Eq. (21) for the three laser intensities. The PIC results are in good agreement with theory. As noted in the previous section, the discrepancy between numerical and theoretical energy depletion rate observed at higher laser intensities can be

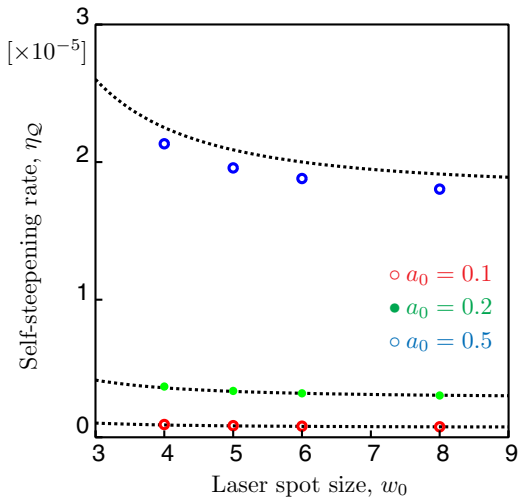

FIG. 2. (Color online) Initial energy depletion rate, $\eta_{\mathcal{Q}}$, as a function of the laser spot, w_0, for different values of the normalized laser strength, $a_0 = 0.1$ (red circles), $a_0 = 0.2$ (green dots), and $a_0 = 0.5$ (blue circles). The longitudinal laser profile is Gaussian with $L = 2$, and $k_0/k_p = 20$. The black dotted lines are the theoretical predictions Eq. (21).

ascribed to the fact that the linear description for the wake amplitude loses its validity.

C. Laser intensity centroid velocity

The normalized-intensity-weighted laser centroid position, ζ_i, is defined as

$$\zeta_i = \frac{\int d\zeta \int dr\, r\zeta |\hat{a}|^2}{\int d\zeta \int dr\, r|\hat{a}|^2} = \frac{1}{\mathcal{Q}} \int d\zeta \int dr\, r\, \zeta |\hat{a}|^2, \tag{22}$$

and the laser intensity centroid velocity, β_i, is given by

$$\beta_i - 1 = \frac{d\zeta_i}{ds}. \tag{23}$$

By using the operatorial expansion Eq. (6) in Eq. (22), and assuming that, initially, $\zeta_i = 0$, we obtain the following expression valid at early times of the laser-plasma interaction for the laser intensity centroid velocity:

$$\beta_i - 1 \simeq -\frac{1}{\mathcal{Q}_0} \frac{k_p^2}{2k_0^2} \int d\zeta \int dr\, r \times \left[\rho \left(2|\hat{a}|^2 + \zeta \frac{\partial |\hat{a}|^2}{\partial \zeta} \right) + \frac{\partial \hat{a}}{\partial r} \frac{\partial \hat{a}^*}{\partial r} \right]. \tag{24}$$

Note that Eq. (24) is valid for any laser intensity. The last term in the integral, which is not multiplied by ρ, is the contribution to laser velocity due to laser diffraction. The initial value of the laser intensity centroid velocity, $\beta_{i,0}$, computed choosing for $\hat{a}$ the Gaussian laser envelope defined in Eq. (5) is

$$\beta_{i,0} - 1 = -\frac{k_p^2}{k_0^2} \left\{ \left[\int d\zeta\, f^2 \right]^{-1} \int_0^\infty du\, e^{-u} \times \int d\zeta\, \rho\left(\zeta, w_0 \sqrt{\frac{u}{2}} \right) [f^2 + \zeta f \partial_\zeta f] + \frac{1}{w_0^2} \right\}. \tag{25}$$

An analytical expression for the initial laser intensity centroid velocity can be obtained in the weakly relativistic regime for a Gaussian laser pulse matched into a parabolic plasma channel. In this case, using Eq. (7) for the proper density, where $\delta\rho$ is given by Eq. (9), and choosing, as before, $f(\zeta) = \exp(-\zeta^2/L^2)$, we obtain

$$\beta_{i,0} - 1 \simeq -\frac{k_p^2}{2k_0^2} \left(1 + \frac{4}{w_0^2} \right) \times \left\{ 1 - a_0^2 \frac{\sqrt{2}}{16} L \left[\frac{3}{2} \mathcal{P}_0(L) - \mathcal{P}_2(L) \right] \right\}, \tag{26}$$

where $\mathcal{P}_m(L) = \int_0^\infty dx\ \sin(xL) x^m \exp(-x^2)$. We note that the factor $(1 + 4/w_0^2)$ is the contribution to the laser velocity coming from the channel, while the term in the curly brackets is the contribution from the laser-induced wakefield. For a very short pulse, $L \ll 1$, we have $\mathcal{P}_m(L) \simeq L\Gamma(m/2+1)/2$, where $\Gamma(x)$ is the gamma function. In this limit, the intensity transport velocity reads

$$\beta_{i,0} - 1 \simeq -\frac{k_p^2}{2k_0^2} \left(1 + \frac{4}{w_0^2} \right) \left(1 - \frac{\sqrt{2}}{64} L^2 a_0^2 \right). \tag{27}$$

For a very long pulse, $L \gg 1$ (adiabatic limit), we have that $\mathcal{P}_0 \simeq 1/L$ and $\mathcal{P}_2(L) \simeq -2/L^3$, and so

$$\beta_{i,0} - 1 \simeq -\frac{k_p^2}{2k_0^2} \left(1 + \frac{4}{w_0^2} \right) \left(1 - \frac{3\sqrt{2}}{32} a_0^2 \right). \tag{28}$$

For a resonant pulse, $L = 2$, the coefficients $\mathcal{P}_m$ can be computed numerically, and we obtain

$$\gamma_{i,0} \simeq \frac{k_0}{k_p} \left(1 + \frac{4}{w_0^2} \right)^{-1/2} \left(1 + 0.05 a_0^2 \right), \tag{29}$$

where we introduced the Lorentz factor for the velocity, namely $\gamma_{i,0} = (1 - \beta_{i,0}^2)^{-1/2}$. The intensity transport velocity grows linearly with the laser intensity for $a_0^2 \ll 1$, with the coefficient determined by the specific longitudinal and transverse laser profile. In the limit of a very broad pulse (and channel), $w_0^2 \gg 4$, the Lorentz factor of the intensity transport velocity is $\gamma_{i,0}^{(\text{3D, broad pulse})} \simeq (k_0/k_p)(1 + 0.05 a_0^2)$. We note that the coefficient that determines, in 3D, and in the broad pulse limit, the dependence of the centroid velocity from laser intensity differs from that in the 1D case [8], where $\gamma_{i,0}^{(\text{1D})} \simeq (k_0/k_p)(1 + 0.1 a_0^2)$. As in the case of the laser energy depletion rate, the difference between 1D and 3D broad pulse limit results can be ascribed to the transverse laser envelope effect.

We compared the prediction for the initial intensity transport velocity Eq. (29) with quasistatic PIC results obtained with the code INF&RNO. Numerical results are presented in Fig. 3, where we show the Lorenz factor of the initial intensity transport velocity as a function of the laser spot, w_0, for different values of the normalized laser strength: $a_0 = 0.1$ (red circles), $a_0 = 0.2$ (green dots), $a_0 = 0.5$ (blue circles), and $a_0 = 0.8$ (purple dots). The longitudinal laser profile is Gaussian with $L = 2$, and $k_0/k_p = 20$. The black dotted lines are the theoretical predictions Eq. (29) for the four laser

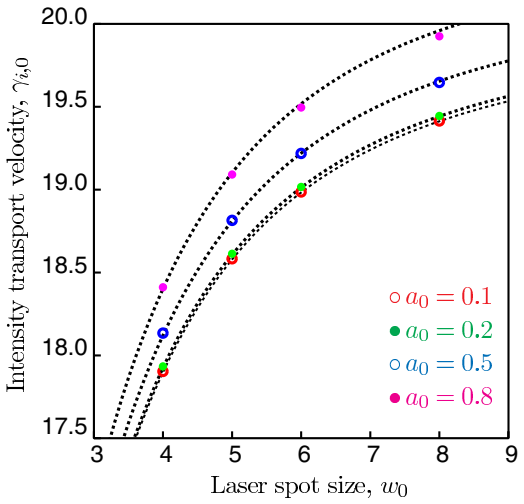

FIG. 3. (Color online) Lorenz factor of the initial intensity transport velocity, $\gamma_{i,0}$, as a function of the laser spot, w_0, for different values of the normalized laser strength, $a_0 = 0.1$ (red circles), $a_0 = 0.2$ (green dots), $a_0 = 0.5$ (blue circles), and $a_0 = 0.8$ (purple dots). The longitudinal laser profile is Gaussian with $L = 2$, and $k_0/k_p = 20$. The black dotted lines are the theoretical predictions Eq. (29).

intensities. The PIC results are in excellent agreement with theory.

IV. PHASE VELOCITY OF LASER-DRIVEN PLASMA WAVES

In this section we present analytical expressions, valid in 3D and in the weakly relativistic limit, for the initial value of the wake phase velocity generated by a short laser pulse with a longitudinal and transverse Gaussian intensity profile (linearly) matched in a parabolic plasma channel. Analytical results are compared with numerical results. We also discuss evolution of the phase velocity during the laser-plasma interaction, showing its dependence on the details of longitudinal and transverse driver evolution.

A. Initial value of the wake phase velocity

In this section we compute, as an example, the phase velocity of the "back" of the first plasma wave period, corresponding to the on-axis point behind the laser driver (i.e., where the laser field is negligible) where the longitudinal wakefield is equal to zero. The velocity of any other phase (e.g., location of the maximum of the longitudinal wakefield, etc.) can be computed in a similar manner. We notice that, in general, the value of phase velocity depends on the chosen wake phase. However, in the weakly relativistic regime, where the nonlinear dependence of plasma wavelength on laser intensity can be neglected, the phase velocity of any point behind the laser driver is independent of the wake phase.

Let us denote by $E_z(\zeta,r,s)$ the longitudinal wakefield generated by the laser after a propagation distance s. We denote by $\zeta_p(s)$ the value of the phase for which we want to compute the velocity. In our example $\zeta_p(s)$ satisfies $E_z[\zeta_p(s),r = 0,s] = 0$ (zero crossing of the longitudinal wakefield). At later times, $s' = s + \Delta s$, with $\Delta s \ll 1$, the phase of the zero crossing will be $\zeta_p(s + \Delta s) \simeq \zeta_p(s) + [\beta_p(s) - 1]\Delta s$, where $\beta_p(s)$ is the value of the phase velocity for the phase $\zeta_p(s)$. Since we are interested in tracking the phase of the zero crossing of the longitudinal wakefield, we have, by definition, $E_z[\zeta_p(s + \Delta s),r = 0,s + \Delta s] = 0$. By considering the Taylor expansion of the latter expression with respect to Δs, and by taking the limit $\Delta s \to 0$, we obtain the following expression for the phase velocity of the zero crossing of the longitudinal wakefield,

$$\beta_p - 1 = -\frac{\partial_s E_z}{\partial_\zeta E_z}\bigg|_{\zeta=\zeta_p,r=0} = -\frac{\partial^2_{\zeta,s}\psi}{\partial^2_{\zeta,\zeta}\psi}\bigg|_{\zeta=\zeta_p,r=0}, \tag{30}$$

where we have introduced the wake potential, ψ, such that $E_z = -\partial_\zeta \psi$. Similarly, denoting by $\zeta'_p(s)$ the phase location of the maximum of E_z behind the laser driver (i.e., $\partial_\zeta E_z|_{\zeta=\zeta'_p,r=0} = 0$), an expression for the (on-axis) phase velocity of the maximum of the longitudinal field is given by

$$\beta'_p - 1 = -\frac{\partial^2_{\zeta,s} E_z}{\partial^2_{\zeta,\zeta} E_z}\bigg|_{\zeta=\zeta'_p,r=0} = \frac{\partial^3_{\zeta,\zeta,s}\psi}{\partial^3_{\zeta,\zeta,\zeta}\psi}\bigg|_{\zeta=\zeta_p,r=0}. \tag{31}$$

We note that Eqs. (30) and (31) are valid for any laser intensity. An explicit evaluation of the phase velocity for any given propagation distance requires the knowledge of the functional dependence of the longitudinal wakefield (or wake potential) on spatial coordinates, ζ and r, and propagation distance, s. Neglecting the transient phase at the early stages of the laser-plasma interaction where the wake is being formed, the wake potential as a function of the driver properties can be evaluated via the quasistatic approximation. Its variation as a function of the propagation distance is determined via Eq. (6), which describes the evolution of the laser driver.

An analytical expression for the phase velocity can be obtained in the weakly relativistic regime. Assuming a broad plasma channel, and using the quasistatic approximation, the wake potential is given by [1]

$$\frac{\partial^2\psi}{\partial\zeta^2} + 1 = \frac{|\hat{a}|^2}{4}, \tag{32}$$

where $|\hat{a}|^2 < 1$. The Green function solution to Eq. (32) is

$$\psi(\zeta,r,s) = -\int_\zeta^\infty d\zeta' \sin(\zeta - \zeta')|\hat{a}(\zeta',r,s)|^2/4, \tag{33}$$

yielding the following expression for the longitudinal wakefield:

$$E_z(\zeta,r,s) = \int_\zeta^\infty d\zeta' \cos(\zeta - \zeta')|\hat{a}(\zeta',r,s)|^2/4. \tag{34}$$

The phase of the on-axis point behind the laser driver where the longitudinal wakefield vanishes, ζ_p, is then given by

$$\int_{-\infty}^{+\infty} d\zeta' \cos(\zeta_p - \zeta')|\hat{a}(\zeta',0,s)|^2 = 0, \tag{35}$$

where we replaced ζ_p with $-\infty$ in the lower integration extreme owing to the fact that we are considering phases behind the driver where the laser field is negligible. By using

Eqs. (30) and (33), the phase velocity of the zero crossing of E_z reads

$$\beta_p - 1 = \frac{\int_{\zeta_p}^{\infty} d\zeta' \cos(\zeta_p - \zeta')\partial_s|\hat{a}(\zeta', r=0, s)|^2}{\int_{\zeta_p}^{\infty} d\zeta' \sin(\zeta_p - \zeta')|\hat{a}(\zeta', r=0, s)|^2}. \quad (36)$$

At early times, the term $\partial_s|\hat{a}|^2$ in the numerator of Eq. (36) can be evaluated by using the operatorial expansion Eq. (6), we have

$$\frac{\partial|\hat{a}|^2}{\partial s} \simeq -\frac{i}{2}\frac{k_p}{k_0}[\hat{a}\nabla_\perp^2\hat{a}^* - \hat{a}^*\nabla_\perp^2\hat{a}] + \frac{k_p^2}{2k_0^2}\left[2\frac{\partial\rho}{\partial\zeta}|\hat{a}|^2 + \rho\frac{\partial|\hat{a}|^2}{\partial\zeta} - \left(\hat{a}\nabla_\perp^2\frac{\partial\hat{a}^*}{\partial\zeta} + \hat{a}^*\nabla_\perp^2\frac{\partial\hat{a}}{\partial\zeta}\right)\right]. \quad (37)$$

At $s = 0$, for the Gaussian laser envelope given in Eq. (5), and choosing $f(\zeta) = \exp(-\zeta^2/L^2)$, with $L \sim 1$, we have that the expression for the phase location of the zero crossing Eq. (35) becomes

$$\cos\zeta_p = 0. \quad (38)$$

Equation (38) has multiple solutions. For a short laser pulse the solution corresponding to the phase location of the zero crossing of E_z at the back of the first plasma wave period is $\zeta_p = -3\pi/2$. We note that at this phase location the field of the (short) laser driver is negligible. Since the initial envelope given in Eq. (5) satisfies $\hat{a} = \hat{a}^*$, Eq. (37) takes the following simplified form for $r = 0$:

$$\left.\frac{\partial|\hat{a}|^2}{\partial s}\right|_{s=0,r=0} \simeq \frac{k_p^2}{k_0^2}a_0^2 e^{-2\zeta^2/L^2} \times \left[\frac{\partial\delta\rho_0}{\partial\zeta} - \frac{2\zeta}{L^2}\left(1 + \frac{4}{w_0^2} + \delta\rho_0\right)\right], \quad (39)$$

where we used Eq. (7) for the proper density, and $\delta\rho_0$ is given by Eq. (9) evaluated at $r = 0$. By using Eqs. (5), (38), and (39) in Eq. (36), we obtain the following expression, valid in the weakly relativistic regime, for the initial value of the phase velocity ($\beta_{p,0}$) of a wake generated by a bi-Gaussian laser driver matched in a parabolic plasma channel,

$$\beta_{p,0} - 1 \simeq -\frac{k_p^2}{2k_0^2}\left[1 + \frac{4}{w_0^2} - \frac{a_0^2}{2}\mathcal{K}(L)\left(1 + \frac{8}{w_0^2}\right)\right], \quad (40)$$

where the function $\mathcal{K}(L)$, which depends on the driver length, is defined as

$$\mathcal{K}(L) = \frac{e^{L^2/16}}{\sqrt{2}}\left[\frac{1}{L^2}\int_0^\infty dx\, x\, \sin x\, \sin\frac{x}{2}e^{-x^2/L^2} + \frac{1}{4}\int_0^\infty dx\, \sin x\, \cos\frac{x}{2}e^{-x^2/L^2} - \int_0^\infty dx\, \cos x\, \sin\frac{x}{2}e^{-x^2/L^2}\right]. \quad (41)$$

For a short laser pulse, $L \ll 1$, $\mathcal{K}(L) \simeq L^2/(8\sqrt{2})$. For a resonant laser pulse, $\mathcal{K}(L = 2) \simeq 0.3853$, and so the Lorentz factor of the initial phase velocity reads

$$\gamma_{p,0} \simeq \frac{k_0}{k_p}\left(1 + \frac{4}{w_0^2}\right)^{-1/2}\left[1 + 0.1\,a_0^2\left(1 + \frac{4}{w_0^2}\right)\right]. \quad (42)$$

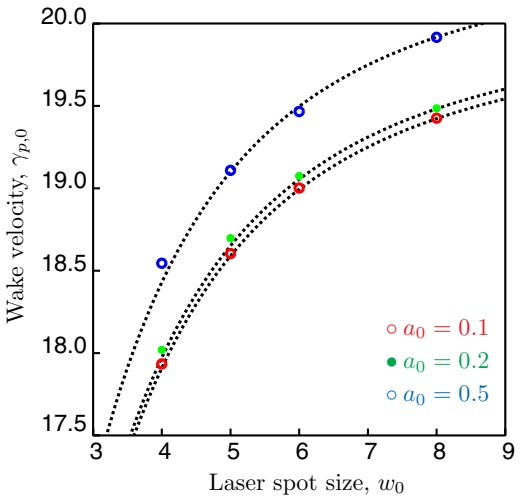

FIG. 4. (Color online) Lorenz factor of the initial wake velocity, $\gamma_{p,0}$, as a function of the laser spot, w_0, for different values of the normalized laser strength, namely $a_0 = 0.1$ (red circles), $a_0 = 0.2$ (green dots), and $a_0 = 0.5$ (blue circles). The longitudinal laser profile is Gaussian with $L = 2$, and $k_0/k_p = 20$. The black dotted lines are the theoretical predictions Eq. (42).

Note that in the limit of a broad pulse, $w_0^2 \gg 4$, the 3D expression for the wake velocity Eq. (42) reduces to the 1D result [8]. We also note that while in 1D, and in the weakly relativistic limit, the wake phase velocity is approximately the intensity transport velocity; this is not the case in 3D. This difference can be ascribed to the fact that in 3D the intensity transport velocity is defined via an integration over the whole (i.e., longitudinal and transverse) laser domain, while, as shown in Eq. (36), the phase velocity of the wake depends on the on-axis ($r = 0$) behavior of the laser driver.

We compared the prediction for the wake phase velocity Eq. (42) with quasistatic PIC results obtained with the code INF&RNO. Numerical results are presented in Fig. 4, where we show the Lorenz factor of the initial wake velocity as a function of the laser spot, w_0, for different values of the normalized laser strength: $a_0 = 0.1$ (red circles), $a_0 = 0.2$ (green dots), and $a_0 = 0.5$ (blue circles). The longitudinal laser profile is Gaussian with $L = 2$, and $k_0/k_p = 20$. The black dotted lines are the theoretical predictions Eq. (42) for the three laser intensities. The PIC results are in excellent agreement with theory.

B. Evolution of the phase velocity

As the laser evolves, so do the plasma wave and its phase velocity. In 3D, the laser driver can evolve longitudinally or transversally. Longitudinal evolution (present also in 1D) is due to self-steepening, depletion and redshifting (i.e., energy exchange with the plasma). Transverse evolution is present every time that, slice-by-slice along the pulse, the guiding contribution from the channel, plasma-wave guiding, self-focusing, and laser diffraction are not exactly balanced. Longitudinal and transverse laser driver evolution are characterized by different characteristic length scales. This can be shown by performing a scale-length analysis of

the laser envelope evolution equation (3). We find that the longitudinal driver evolution occurs over a propagation length $L_{\rm long} \sim k_0^2/k_p^2$ (assuming a short laser pulse, $L \sim 1$), while transverse evolution usually happens over a typically shorter length scale, $L_{\rm trans} \sim (k_0/k_p) r_\perp^2$, where $r_\perp$ is the characteristic transverse size of the laser. As a consequence, for laser-plasma parameters of interest for current and future LPA experiments, and for propagation distances shorter than the depletion length, the evolution of the phase velocity will be sensitive to the details of the transverse evolution of the laser driver (e.g., position of the laser focus in the plasma, laser mode properties, contributions from self-focusing and plasma-wave guiding, etc.).

To illustrate the laser and wake evolution we consider the propagation of a short and moderately intense, bi-Gaussian laser pulse in parabolic plasma channel. The laser envelope is the one defined in Eq. (5), with $a_0 = 0.5$, $w_0 = 4$, $f(\zeta) = \exp(-\zeta^2/L^2)$, and $L = 2$. The laser is linearly matched in the channel, and $k_0/k_p = 20$. The modeling of the laser-plasma interaction has been done with the quasistatic PIC code INF&RNO. The use of a quasistatic code allows us to neglect the initial transient corresponding to the generation of the wake, which depends on the details of the incoupling geometry. The evolution during laser propagation of the wake phase velocity, measured at the back of the first plasma period, at the location of the zero crossing of the longitudinal electric field E_z, is shown in Fig. 5 (black solid line). The black dashed curve in Fig. 5 is the evolution of the normalized-intensity-weighted laser radius, defined as $\overline{w}(s) = [2 \int d\zeta \int r\, dr\, r^2 |\hat{a}|^2/\mathcal{Q}]^{1/2}$.

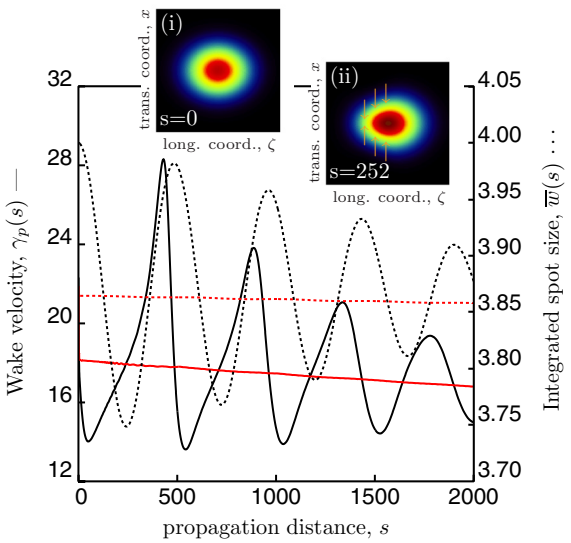

FIG. 5. (Color online) Evolution of the wake phase velocity, $\gamma_p(s)$ (black solid line), and normalized-intensity-weighted laser radius $\overline{w}(s)$ (black dashed line), for a Gaussian laser driver with $a_0 = 0.5$, $w_0 = 4$, and $f(\zeta) = \exp(-\zeta^2/L^2)$ with $L = 2$. The laser is linearly matched in a parabolic plasma channel, and $k_0/k_p = 20$. The two insets show snapshots of the laser envelope for two propagation distances: (i) $s = 0$ and (ii) $s = 252$, illustrating the compression of the laser driver in the region towards the back of the pulse. The red solid line and the red dashed line show, respectively, the evolution of the wake phase velocity and laser radius for a "supermatched" driver.

With this definition, $\overline{w}(s = 0) = w_0$. As the laser propagates, different longitudinal slices along the laser driver experience different amounts of self-focusing and plasma-wave guiding. In particular, the slices towards the front of the laser pulse are well matched in the parabolic plasma channel since the additional contribution to guiding coming from self-focusing is canceled by plasma response, while the slices towards the back of the laser driver experience enhanced focusing compared to those in the front. In fact, for $s \lesssim 250$, $\overline{w}(s)$ decreases. The two insets in Fig. 5 show snapshots of the laser envelope for two propagation distances, (i) $s = 0$, and (ii) $s = 252$, illustrating the compression of the laser driver in the region towards the back of the pulse.

Owing to the transverse redistribution of the laser energy, the on-axis intensity profile is also changed. Initially, the on-axis laser intensity is Gaussian, at later times it becomes longitudinally asymmetric, with the location of the intensity peak slipping back compared to $s = 0$. This change in the laser intensity profile induces a change in the lineout of the longitudinal wakefield, with the position of the zero crossing of the E_z shifting progressively towards the back (more negative phases) as the propagation distance approaches $s \simeq 250$. This is the reason why the phase velocity, whose initial value is given by $\gamma_{p,0} \simeq 18.5$ [see Eq. (42)], is always slower than the initial value for $s \lesssim 250$. The minimum value of the phase velocity, $\gamma_{p,\rm min} \simeq 14$, is reached for $s \simeq 50$. At $s \simeq 250$ the driver reaches the maximum compression, and, afterwards, for $250 \lesssim s \lesssim 500$, the back of the laser driver expands and the initial laser envelope configuration is (almost) recovered at $s \simeq 500$. During this time span the location of the zero crossing of E_z moves forward, giving a value for the phase velocity that is consistently higher than the initial one. The maximum value of the phase velocity, $\gamma_{p,\rm max} \simeq 28$, is reached for $s \simeq 430$. For $s \gtrsim 500$ the cycle described repeats. We note that the length over which the phase velocity evolves corresponds to the characteristic scale length for mismatched oscillations in a parabolic plasma channel, $Z_{\rm mismatch} \simeq \pi (k_0/k_p) w_0^2/2 \simeq 500$, which is, in these laser-plasma conditions, the characteristic scale for transverse laser evolution. The damping of the oscillations in both $\overline{w}(s)$ and $\gamma_p(s)$ at later times is due to the fact that a short laser driver, as the one used in this example, is not monochromatic [25]. Each chromatic component of the laser is characterized by a different oscillation frequency, and the decoherence between these modes damps out the oscillations.

Besides the evolution due to transverse laser dynamics, the phase velocity evolves, as in 1D, because of the longitudinal evolution of the driver. In particular, we see that the average value of the phase velocity slowly decreases during laser propagation. As shown in Ref. [8], this is due to laser redshifting (i.e., energy depletion).

To further support the point that the large variations of the phase velocity during the early stages (i.e., for a propagation length short compared to the depletion length) of the laser-plasma interaction are due to transverse laser evolution, we considered a second example replacing the linearly matched Gaussian laser pulse driver with a "supermatched" laser driver, fixing all the other laser-plasma parameters. A supermatched laser pulse (see the Appendix) has a slice-by-slice intensity distribution adjusted such that, on each slice, laser diffraction,

TABLE I. This table compares the 1D and 3D expressions for the initial value of the laser pump depletion, L_{pd}, laser intensity centroid velocity, $\gamma_{i,0}$, and wake phase velocity, $\gamma_{p,0}$, valid in different laser-plasma interaction regimes, namely, linear ($a_0 \ll 1$) and mildly relativistic ($a_0 \lesssim 1$). The expressions assume a resonant Gaussian pulse profile.

	L_{pd}	$\gamma_{i,0}$	$\gamma_{p,0}$
1D ($a_0 \ll 1$)	∞	$\frac{k_0}{k_p}$	$\frac{k_0}{k_p}$
3D ($a_0 \ll 1$)	∞	$\frac{k_0}{k_p}\left(1+\frac{4}{w_0^2}\right)^{-1/2}$	$\frac{k_0}{k_p}\left(1+\frac{4}{w_0^2}\right)^{-1/2}$
1D ($a_0 \lesssim 1$)	$\frac{k_0^2}{k_p^2}\frac{2^{7/2}e}{\pi^{1/2}}\frac{1}{a_0^2}$	$\frac{k_0}{k_p}(1+0.1a_0^2)$	$\frac{k_0}{k_p}(1+0.1a_0^2)$
3D ($a_0 \lesssim 1$)	$\frac{k_0^2}{k_p^2}\frac{2^{9/2}e}{\pi^{1/2}}\frac{1}{a_0^2}\left(1+\frac{4}{w_0^2}\right)^{-1}$	$\frac{k_0}{k_p}\left(1+0.05a_0^2\right)\left(1+\frac{4}{w_0^2}\right)^{-1/2}$	$\frac{k_0}{k_p}\left[1+0.1a_0^2\left(1+\frac{4}{w_0^2}\right)\right]\left(1+\frac{4}{w_0^2}\right)^{-1/2}$

channel guiding, self-focusing, and plasma-wave guiding are perfectly balanced, yielding an intensity distribution that does not change during propagation (for propagation distances much shorter than laser depletion). In this numerical example we are using a supermatched driver of order $q = 0$ (see the Appendix for details), and we use the same parabolic background density profile utilized in the Gaussian example discussed before. As shown by the red dashed line in Fig. 5, the quantity $\overline{w}(s)$ for the supermatched driver simulation is constant. The evolution phase velocity of the wake generated by the supermatched driver is shown by the red solid line in Fig. 5. As expected, since there is no transverse evolution of the driver, the phase velocity does not oscillate. The slow and steady decrease of the phase velocity is due, as in the Gaussian case, to longitudinal evolution of the driver (redshifting and depletion).

V. CONCLUSIONS

In this paper we have investigated the evolution, in 3D, of a moderately intense ($a_0 < 1$) short-pulse ($L \sim 1$) laser propagating in an underdense ($k_p/k_0 \ll 1$) parabolic plasma channel, and that of the associated plasma wave. Understanding the details of the propagation of short and intense laser pulses in plasmas is a topic of fundamental importance in the field of laser-plasma interactions and, in particular, for the design and optimization of LPAs. For instance, the phase velocity of the laser-generated plasma waves determines the trapping threshold for particle self-injection and sets the dephasing length, while the energy depletion rate determines the maximum laser propagation distance. We derived analytical expressions, valid in the early stages of the laser plasma interaction (i.e., before significant depletion takes place), for the laser energy depletion rate, the laser self-steepening rate, the intensity centroid transport velocity, and the wake phase velocity. These quantities are calculated by using an envelope description for the laser pulse and the linearized quasistatic approximation for the plasma response. Analytical results computed for a bi-Gaussian laser pulse matched in a parabolic plasma channel are found to be in excellent agreement with results from PIC simulations performed with the code INF&RNO. A summary of the quantities computed in this paper is shown in Table I, together with the corresponding 1D expressions valid in the linear and in the mildly relativistic regimes. We note that the correct 3D expressions characterizing the laser evolution and the plasma-wave phase velocity cannot be inferred from 1D results. This is due to the interplay between longitudinal and transverse effects in the laser evolution, which, in turn, depends on the details of the laser envelope. In fact, the difference between 1D and 3D results is not simply given by a predetermined geometric factor. For instance, we find that, for a laser pulse with a longitudinal and transverse Gaussian intensity profile in the limit of a very broad pulse, the expression for the energy depletion, self-steepening rate, and intensity transport velocity are different from the corresponding expressions obtained in the 1D case discussed in Refs. [8,12], while the 3D expression for the phase velocity reduces to the 1D case.

We also studied the dependence of the phase velocity on laser driver evolution, identifying and discussing the role of transverse and longitudinal evolution. We found that, in 3D, and for laser-plasma parameters of interest for current and future LPA experiments, the evolution of the phase velocity is mainly determined by the details of the transverse laser evolution, whereas changes in the phase velocity related to longitudinal driver evolution only play a role over propagation distances comparable with the depletion length.

All the results presented in this paper are valid in the weakly relativistic regime, $a_0 \lesssim 1$. The extension of these 3D results to the relativistic regime, $a_0 \gtrsim 1$, will be the subject of future work.

ACKNOWLEDGMENTS

This work was supported by the Director, Office of Science, Office of High Energy Physics, of the U.S. DOE under Contract No. DE-AC02-05CH11231, and used the computational facilities at the National Energy Research Scientific Computing Center (NERSC). The authors would like to thank B. A. Shadwick, S. S. Bulanov, and G. Turchetti for useful discussions and suggestions.

APPENDIX: PERFECT MATCHING OF AN INTENSE, SHORT-PULSE LASER IN A PARABOLIC PLASMA CHANNEL

The laser envelope evolution equation for propagation distances much shorter than the depletion length is given by the paraxial wave equation, which can be obtained from Eq. (3) by dropping the mixed derivative, $\partial^2_{\zeta,s}\hat{a}$,

$$\left(\nabla_\perp^2 + 2i\frac{k_0}{k_p}\frac{\partial}{\partial s}\right)\hat{a} = \rho\hat{a}. \tag{A1}$$

Consider solutions to Eq. (A1) of the form

$$\hat{a}(\zeta,r,s) = a_0 f(\zeta) g(\zeta,r,s) \exp[i\varphi(\zeta,r,s)], \tag{A2}$$

where a_0 is the initial peak amplitude, $f(\zeta)$ describes the longitudinal profile [$f(0) = 1$, and $0 \leqslant f(\zeta) < 1$, for $\zeta \neq 0$], $g(\zeta,r,s)$ describes, for any given longitudinal slice, ζ, the transverse intensity profile, and $\varphi(\zeta,r,s)$ is a phase. We assume that $\int dr\, r[g(\zeta,r,s=0)]^2 = \text{const}$, so the initial longitudinal power profile is determined uniquely by the choice of $f(\zeta)$. By inserting Eq. (A2) into Eq. (A1), we obtain the following set of coupled equations for $g(\zeta,r,s)$ and $\varphi(\zeta,r,s)$:

$$\nabla_\perp^2 g - (\partial_r\varphi)^2 g - 2\frac{k_0}{k_p}(\partial_s\varphi) g = \rho g, \tag{A3}$$

$$g\nabla_\perp^2\varphi + 2(\partial_r\varphi)(\partial_r g) + 2\frac{k_0}{k_p}(\partial_s g) = 0. \tag{A4}$$

A laser pulse propagating in a plasma channel for which the intensity distribution is, slice-by-slice, constant for propagation distances short compared to the depletion length (i.e., laser diffraction, channel focusing, plasma-wave guiding, and self-focusing are perfectly balanced) is said to be "perfectly matched" in the channel (supermatched laser pulse). A quasimatched laser pulse [14], where the intensity distribution at each longitudinal slice is assumed to be Gaussian, and the spot size is ζ dependent, can be considered an approximation of a supermatched pulse. For the laser envelope described in Eq. (A2), a constant intensity distribution during propagation implies $\partial_s g = 0$. Equation (A4) then gives $r(\partial_r\varphi)g^2 = \text{const}$. Taking into account that φ is an even function of r near $r = 0$, and so $(\partial_r\varphi)|_{r=0} = 0$, and assuming that $g(r=0)$ has a finite value, then $\partial_r\varphi = 0$ for any r, and the phase fronts of a supermatched driver are flat. Equation (A3) then becomes

$$\nabla_\perp^2 g - 2\frac{k_0}{k_p}(\partial_s\varphi) g = \rho g. \tag{A5}$$

We can solve Eq. (A5) once boundary (asymptotic) conditions for g are specified. For longitudinal phases, ζ, well ahead of the laser pulse peak, where the laser amplitude and the associated wake are negligibly small, the proper density coincides with the unperturbed (background) plasma density, $\rho = \rho_0$. For a parabolic plasma channel parametrized as $\rho_0 = 1 + 4r^2/R^4$, where R is a constant, possible solutions to Eq. (A5) are given by $g(\zeta,r) = L_q(2r^2/R^2)\exp(-r^2/R^2)$, where $L_q(x)$ is the Laguerre polynomial of order q, as shown in Refs. [1,26]. Similarly, for phases around the laser peak, but in the limit of r very large, where the laser and wakefield amplitudes are negligible, we have, as before, $\rho = \rho_0 = 1 + 4r^2/R^4$. Invoking continuity with the phases ahead, we assume that, asymptotically, $g(\zeta,r) = L_q(2r^2/R^2)\exp(-r^2/R^2)$. Since φ does not depend on r, we can compute the quantity $\partial_s\varphi$ using Eq. (A5) in the limit for large r, where the wakefield vanishes. With the assumptions on the asymptotic behavior of g, we obtain

$$-2\frac{k_0}{k_p}(\partial_s\varphi) = 1 + \frac{4}{R^2}(1+2q). \tag{A6}$$

By inserting the expression for $\partial_s\varphi$ given by Eq. (A6) into Eq. (A5), we can rewrite the equation describing, slice-by-slice, the transverse field amplitude ensuring perfect matching in a parabolic plasma channel as

$$\nabla_\perp^2 g = \left[\rho - 1 - \frac{4}{R^2}(1+2q)\right] g. \tag{A7}$$

Equation (A7) depends on the proper density; hence it must be solved self-consistently together with the equation for the wake amplitude. In particular, in the mildly relativistic regime, we have that $\rho = \rho_0 + \delta\rho = 1 + 4r^2/R^4 + \delta\rho$, with $\delta\rho$ given by Eq. (8), where $|\hat{a}|^2 = a_0^2 f^2 g^2$. In the nonlinear (relativistic) regime the proper density can be evaluated numerically.

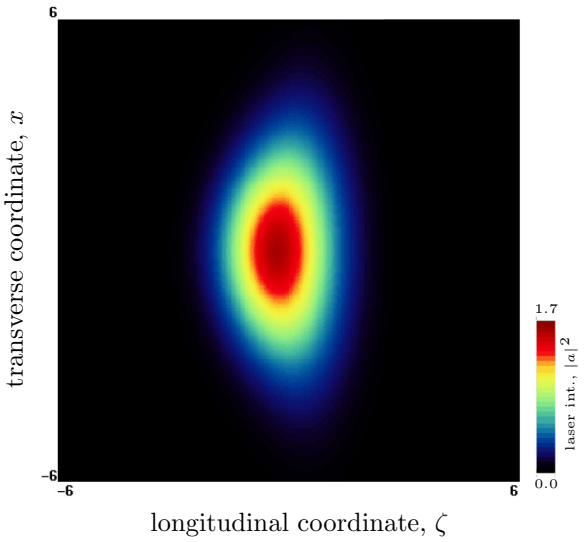

FIG. 6. (Color online) Normalized laser intensity field $|\hat{a}(x, y = 0, \zeta)|$ for a "supermatched" laser pulse driver in a parabolic plasma channel. The form of the laser envelope is given in Eq. (A2), with $a_0 = 1$, and where we choose $f(\zeta) = \exp(-\zeta^2/L^2)$, with $L = 2$. The function $g(\zeta,r)$ is the solution of Eq. (A7) with $q = 0$ and $R = 5$.

An example of supermatched laser profile obtained solving numerically Eq. (A7) for $q = 0$, $a_0 = 1$, $R = 5$, and choosing $f(\zeta) = \exp(-\zeta^2/L^2)$, with $L = 2$, is shown in Fig. 6. We notice that the laser intensity distribution of a supermatched pulse in a parabolic channel has a conical shape (narrower towards the back). Physically this is due to the fact that the slices towards the back of the pulse experience larger plasma-wave guiding compared to the slices in the front, so the laser spot has to shrink to increase diffraction and recover equilibrium.

In the mildly relativistic limit, the phase velocity for the wake generated by a supermatched laser pulse can be computed by using Eq. (36), where the laser envelope is given by Eq. (A2), and using the conditions Eqs. (A6) and (A7) that define the supermatched solution. We obtain the following expression for the wake phase velocity,

$$\beta_p^{\text{supermatched}} - 1 = -\frac{k_p^2}{2k_0^2}\left[1 + \frac{4}{R^2}(1+2q)\right], \tag{A8}$$

and so

$$\gamma_p^{\text{supermatched}} = \frac{k_0}{k_p}\left[1 + \frac{4}{R^2}(1+2q)\right]^{-1/2}. \tag{A9}$$

We see that for $a_0 < 1$ the phase velocity for the wake generated by a supermatched laser pulse is independent

of the laser intensity to order a_0^2, and depends only on the on-axis density, plasma profile, and transverse laser mode (defined via the parameter q). Note that this result differs from that of a Gaussian laser pulse, and in the limit of a broad pulse, $R^2 \gg 4$, we do not recover the 1D limit [8].

[1] E. Esarey, C. B. Schroeder, and W. P. Leemans, Rev. Mod. Phys. **81**, 1229 (2009).

[2] X. Wang, R. Zgadzaj, N. Fazel, Z. Li, S. A. Yi, X. Zhang, W. Henderson, Y.-Y. Chang, R. Korzekwa, H.-E. Tsai, C.-H. Pai, H. Quevedo, G. Dyer, E. Gaul, M. Martinez, A. C. Bernstein, T. Borger, M. Spinks, M. Donovan, V. Khudik, G. Shvets, T. Ditmire, and M. C. Downer, Nat. Commun. **4**, 1988 (2013).

[3] H. T. Kim, K. H. Pae, H. J. Cha, I. J. Kim, T. J. Yu, J. H. Sung, S. K. Lee, T. M. Jeong, and J. Lee, Phys. Rev. Lett. **111**, 165002 (2013).

[4] W. P. Leemans, A. J. Gonsalves, H.-S. Mao, K. Nakamura, C. Benedetti, C. B. Schroeder, C. Tóth, J. Daniels, D. E. Mittelberger, S. S. Bulanov, J.-L. Vay, C. G. R. Geddes, and E. Esarey, Phys. Rev. Lett. **113**, 245002 (2014).

[5] C. Benedetti, C. B. Schroeder, E. Esarey, F. Rossi, and W. P. Leemans, Phys. Plasmas **20**, 103108 (2013).

[6] C. D. Decker and W. B. Mori, Phys. Rev. Lett. **72**, 490 (1994).

[7] W. Lu, M. Tzoufras, C. Joshi, F. S. Tsung, W. B. Mori, J. Vieira, R. A. Fonseca, and L. O. Silva, Phys. Rev. ST Accel. Beams **10**, 061301 (2007).

[8] C. B. Schroeder, C. Benedetti, E. Esarey, and W. P. Leemans, Phys. Rev. Lett. **106**, 135002 (2011).

[9] A. Pukhov and J. Meyer-ter-Vehn, Appl. Phys. B **74**, 355 (2002).

[10] C. Benedetti, C. B. Schroeder, E. Esarey, C. G. R. Geddes, and W. P. Leemans, in *Proceedings of (2010) AAC Workshop*, edited by G. Nusinovich and S. Gold (AIP, NY, 2010), Vol. 1299, pp. 250–255.

[11] C. Benedetti, C. B. Schroeder, E. Esarey, and W. P. Leemans, Efficient Modeling of Laser-plasma Accelerators Using the Ponderomotive-based code INF&RNO, in *Proceedings of the 11th International Computational Accelerator Physics Conference (ICAP), Rostock-Warnemunde, Germany* (JACoW, 2012), p. 206, paper THAII2, http://jacow.org/.

[12] B. A. Shadwick, C. B. Schroeder, and E. Esarey, Phys. Plasmas **16**, 056704 (2009).

[13] A. J. Brizard, Phys. Plasmas **5**, 1110 (1998).

[14] C. Benedetti, C. B. Schroeder, E. Esarey, and W. P. Leemans, Phys. Plasmas **19**, 053101 (2012).

[15] E. Esarey, C. B. Schroeder, B. A. Shadwick, J. S. Wurtele, and W. P. Leemans, Phys. Rev. Lett. **84**, 3081 (2000).

[16] P. Sprangle, E. Esarey, and A. Ting, Phys. Rev. A **41**, 4463 (1990).

[17] P. Sprangle, E. Esarey, and A. Ting, Phys. Lett. **64**, 2011 (1990).

[18] P. Mora and T. M. Antonsen, Phys. Plasmas **4**, 217 (1997).

[19] N. E. Andreev, L. M. Gurbunov, V. I. Kirsanov, K. Nakajima, and A. Ogata, Phys. Plasmas **4**, 1145 (1997).

[20] S. V. Bulanov, I. N. Inovenkov, V. I. Kirsanov, N. M. Naumova, and A. S. Sakharov, Phys. Fluids B **4**, 1935 (1992).

[21] W. Zhu, J. P. Palastro, and T. M. Antonsen, Phys. Plasmas **19**, 033105 (2012).

[22] W. Zhu, J. P. Palastro, and T. M. Antonsen, Phys. Plasmas **20**, 073103 (2013).

[23] D. F. Gordon, B. Hafizi, R. F. Hubbard, J. R. Penano, P. Sprangle, and A. Ting, Phys. Rev. Lett. **90**, 215001 (2003).

[24] J. Vieira, F. Fiuza, L. O. Silva, M. Tzoufras, and W. B. Mori, New J. Phys. **12**, 045025 (2010).

[25] E. Esarey and W. P. Leemans, Phys. Rev. E **59**, 1082 (1999).

[26] C. B. Schroeder, C. Benedetti, E. Esarey, J. van Tilborg, and W. P. Leemans, Phys. Plasmas **18**, 083103 (2011).